Mon. Not. R. Astron. Soc. **358,** 632–640 (2005) doi:10.1111/j.1365-2966.2005.08805.x

Modelling the photopolarimetric variability of AA Tau

Mark O'Sullivan,[1⋆] Michael Truss,[1] Christina Walker,[1] Kenneth Wood,[1] Owen Matthews,[2] Barbara Whitney[3] and J. E. Bjorkman[4]

[1]*School of Physics & Astronomy, University of St. Andrews, North Haugh, St Andrews KY16 9SS*
[2]*Laboratory for Astrophysics, Paul Scherrer Institute, Wurenlingen und Villigen, CH-5232, Villigen PSI, Switzerland*
[3]*Space Science Institute, 3100 Marine Street, Suite A353, Boulder CO 80303, USA*
[4]*Ritter Observatory, Department of Physics & Astronomy, University of Toledo, Toledo OH 43606, USA*

Accepted 2005 January 10. Received 2005 January 7; in original form 2004 June 15

ABSTRACT

We present Monte Carlo scattered light models of a warped disc that reproduce the observed photopolarimetric variability of the classical T Tauri star, AA Tauri. For a system inclination of 75° and using an analytic description for a warped inner disc, we find that the shape and amplitude of the photopolarimetric variability are reproduced with a warp that occults the star, located at 0.07 au, amplitude 0.016 au, extending over radial and azimuthal ranges 0.0084 au and 145°. We also show a time sequence of high spatial resolution scattered light images, showing a dark shadow cast by the warp sweeping round the disc. Using a modified smooth particle hydrodynamics code, we find that a stellar dipole magnetic field of strength 5.2 kG, inclined at 30° to the stellar rotation axis can reproduce the required disc warping to explain the photopolarimetric variability of AA Tau.

Key words: circumstellar matter – stars: individual: AA Tau.

1 INTRODUCTION

Observationally, pre-main-sequence T Tauri stars may be divided into classical and weak T Tauri stars (cTTS and wTTS, respectively; Appenzeller & Mundt 1989; Bertout 1989). The cTTS exhibit broad Hα indicative of on-going accretion and are surrounded by large dusty discs inferred from their signature infrared (IR) excess emission. On the other hand, wTTS do not exhibit the strong Hα and large IR excesses, and these systems may have ceased accreting and have very low mass discs. Both cTTS and wTTS exhibit photometric variability (a defining feature of T Tauri stars; Joy 1945), with wTTS exhibiting periodic and cTTS quasi-periodic variability (Appenzeller & Mundt 1989; Bertout 1989). Hot and cool spots on the stellar surface are believed to be responsible for the variability, with long-lived cool spots dominant in wTTS (Hatzes 1995) and short-lived hotspots, possibly linked to the accretion process, dominating in cTTS (Bouvier et al. 1993; Herbst et al. 1994; Kenyon et al. 1994; Eaton, Herbst & Hillenbrand 1995; Choi & Herbst 1996). The currently popular magnetospheric accretion model predicts hotspots on the stellar surface (Ghosh & Lamb 1979; Koenigl 1991; Shu et al. 1994). In this model, a stellar dipole magnetic field threads, truncates and possibly warps the circumstellar disc. Disc material is accreted on to the star along magnetic field lines forming hotspots or rings on the stellar surface at the magnetic poles (Mhadavi & Kenyon 1998).

⋆E-mail: mo5@st-andrews.ac.uk

The magnetospheric accretion model has been applied to explain the photometric variability in the cTTS system DR Tauri (Kenyon et al. 1994). For the edge-on disc around HH 30 IRS, variability has been observed in both *Hubble Space Telescope* (*HST*) images (Burrows et al. 1996; Stapelfeldt et al. 1999; Cotera et al. 2001) and ground based *VRI* photometry (Wood et al. 2000). The variability in HH 30 IRS has been modelled as a result of hotspots (Wood & Whitney 1998; Wood et al. 2000) and a disc warp (Stapelfeldt et al. 1999), but no period has so far been determined. Photopolarimetric variability has recently been observed in the cTTS AA Tauri (Bouvier et al. 1999, 2003) and has been interpreted as the result of occultation of a star by a warp in the inner regions of a circumstellar disc. The variability is found to have a period of 8.2 d, but the variations sometimes turn-off, possibly as a result of non-steady accretion.

In this paper, we extend our Monte Carlo photopolarimetry simulations of systems with hot star spots (Wood et al. 1996; Wood & Whitney 1998; Stassun & Wood 1999) to include the effects of disc warps. We construct a warped disc model that reproduces the photopolarimetric variability of AA Tau. Then, using a modified smoothed particle hydrodynamics (SPH) code incorporating forces from an inclined dipole stellar magnetic field, we explore the magnetic field strength and configuration required to warp the AA Tau disc and reproduce the observed photopolarimetric variability. Section 2 describes the photopolarimetric data. Section 3 presents models for the system using the spectral energy distribution (SED) to constrain the large-scale disc structure and photopolarimetric variability to constrain the warping of the inner disc; we also present

a time sequence of high spatial resolution scattered light images. Section 4 presents our SPH simulations of a disc with an inclined stellar dipole field and we summarize our results in Section 5.

2 AA TAU PHOTOPOLARIMETRY

The photopolarimetry of AA Tau has been reported in a number of studies. The young star at the heart of the system has been classified as a K7 (Kenyon & Hartmann 1995), with a mass of 0.8 $M_\odot$, radius of 1.85 $R_\odot$ and an effective temperature of 4030 ± 30 K (Bouvier et al. 1999). From analysis of the photometric variability the disc of the system, inferred from the IR excess emission (e.g. D'Alessio et al. 1999), is estimated to be at an inclination of 70° or greater (Bouvier et al. 1999). The observed photometric variability is achromatic and is attributed to occultation of the star by a warp in the inner disc (Terquem & Papaloizou 2000; Bouvier et al. 2003). The occultation results in $\Delta V \sim 1$ mag, has a duration of around 3–4 d and recurs every 8.2 d, but occasionally an occultation event is missing. Observations show the overall brightness level and depth of eclipses are variable (Bouvier et al. 2003), suggestive of stochastic magnetospheric accretion in AA Tau. Throughout this study the time-averaged photopolarimetric variations given here are used as the basis for the model. Assuming a Keplerian disc, the warp responsible for the periodic occultation must be located at 0.07 au (Bouvier et al. 2003).

Polarimetry studies show that the linear polarization increases as the observed flux decreases and that the polarization has a range of 0.6–1.3 per cent (Menard et al. 2003). The polarization position angle is shown to vary from 0° to almost 30° (Bouvier et al. 1999) and studies of nearby stars exhibit similarly large position angle variations. The large position angle variations are attributed to interstellar polarization of around 0.5 per cent, so the intrinsic polarization is variable in the range ∼0.1–0.8 per cent (Menard et al. 2003).

3 RADIATION TRANSFER MODELS

We model the SED and photopolarimetry of AA Tau using our suite of Monte Carlo scattered light and radiative equilibrium codes. For the SED models, we use an axisymmetric disc to determine the disc shape and mass. The photopolarimetric modelling uses a non-axisymmetric warped inner disc described below.

As we model the time-dependent photopoalrimetry with a warped disc, a fully self-consistent model should calculate the 3D time-dependent disc temperature and density structure and time-dependent SED. Such a calculation is beyond the scope of this paper and instead we present three separate models. The first models the SED of AA Tau with an axisymmetric disc. The disc structure is calculated by enforcing vertical hydrostatic equilibrium in the disc as described in Walker et al. (2004). In the second model, we model the photopolarimetry using an analytic description for warping of the inner disc and for the outer disc we use the hydrostatic disc structure derived from the SED modelling. We use the height and shape of the warp from these analytic models as a guide for our dynamical models of the interaction of a disc with a dipole stellar magnetic field. We present the resulting photopolarimetry from this model, again using the disc structure derived from SED models for the outer disc.

We do not expect the time-dependent 3D disc structure (as a result of shadowing of different regions of the outer disc by the warp) to effect our simulated photometric variability. The photometric variability is primarily produced by occultations of the star and the contribution from scattered starlight in the outer disc is small. However, the shape of the outer disc may be important for accurately modelling the polarimetric variability because it is produced by the scattering of starlight. We plan to explore three dimensional disc structure models in the future. In the meantime, we proceed with the modelling as outlined above and detailed below.

3.1 Disc structure from SED modelling

The spectral energy distribution of AA Tau exhibits the large IR excess emission characteristic of dusty protoplanetary discs. We model the SED with our Monte Carlo radiative equilibrium techniques (Bjorkman & Wood 2001; Wood et al. 2002; Whitney et al. 2003) updated to include an iterative loop to calculate the disc structure for an irradiated steady accretion disc in vertical hydrostatic equilibrium (Walker et al. 2004). This approach follows D'Alessio et al. (1999) in adopting Shakura & Sunyaev (1973) α-disc theory to describe cTTS accretion discs. Therefore, the disc density is not parametrized by power laws as in our previous SED models (e.g. Wood et al. 2002; Rice et al. 2003). In our simulations, we adopt the dust opacity model, which we have used to successfully model the SEDs of the HH 30 IRS and GM Aur discs (Wood et al. 2002; Rice et al. 2003; Schneider et al. 2003). The wavelength dependence of this dust opacity is displayed in Wood et al. (2002, fig. 2) and has $\kappa_B/\kappa_K = 2.5$, which is in the range of good fits as determined from the scattered light models of the HH 30 IRS disc using parametric disc models (Watson & Stapelfeldt 2004). The optical dust scattering properties (opacity, κ, albedo, a, phase function asymmetry parameter, g, and maximum polarization, P) are shown in Table 1. These parameters are incorporated into our scattered light models as described in Code & Whitney (1995).

Our iterative Monte Carlo radiative equilibrium code self-consistently calculates the disc density and temperature structure and emergent spectrum at a range of viewing angles. From consideration of the photopolarimetric variability, the inclination of AA Tau has been estimated to be around 70°. Our simulations show that we can reproduce the AA Tau SED at a viewing angle of $i \sim 70°$ with the following parameters $T_\star = 4000$ K, $R_\star = 1.9$ $R_\odot$, $R_{\rm d} = 150$ au and $\dot{M} = 7.5 \times 10^{-9}$ $M_\odot$ yr^{-1}, corresponding to a total disc mass of $M_{\rm d} = 0.02$ $M_\odot$. The code calculates an inner radius for the disc of $7R_\star$, corresponding to our adopted dust destruction temperature of 1600 K.

Fig. 1 shows observations of AA Tau and our SED model for the system described above, viewed at $i = 65°$, 68° and 71°. Observations come from the Kenyon & Hartmann (1995) compilation (squares) with additional *(ISO) Infrared Space Observatory* fluxes (triangles) from Chiang et al. (2001). The input stellar spectrum is from a Kurucz model atmosphere (Kurucz 1995). For inclinations $i > 70°$, the direct optical starlight becomes obscured by the flared disc. Therefore, if the system inclination is indeed greater than 70°, this points to some potential shortcomings in our models. For example, some dust settling could effectively reduce the disc scaleheight and therefore allow the star to be viewed at inclinations $i > 75°$

Table 1. Dust properties.

	κ (cm^{-2} g^{-1})	a	g	P (per cent)
U	46.2	0.47	0.64	39.3
B	42.3	0.48	0.63	41.1
V	37.5	0.49	0.62	40.6
I	28.9	0.52	0.60	38.1

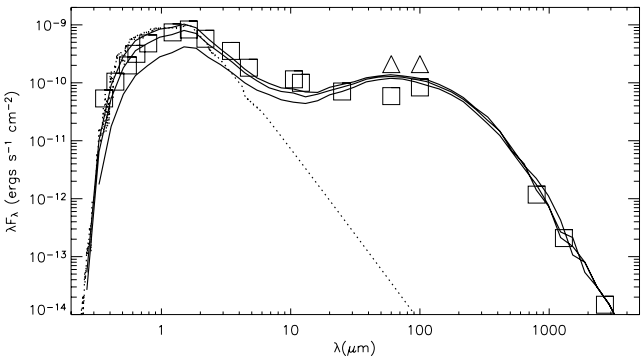

Figure 1. Spectral energy distribution data and model for AA Tau. The dotted line is the adopted input stellar spectrum and the three solid lines are the model SEDs for inclinations of (from top to bottom) 65°, 68° and 71°. The different data points at 60 and 100 μm represent *IRAS* (squares) and *ISO* (*Infrared Space Observatory*; triangles) observations.

(e.g. Dullemond & Dominik 2004). We have not attempted to fit the optical flux, because that is observed to vary and is the subject of the next section. The point of this SED model is to obtain estimates for the disc mass and density structure based on a physically plausible disc model. We then use this as the outer disc structure in our subsequent optical scattered light models that use a warped inner disc. Future work will investigate the effects of dust settling on the SED and inclination determinations.

3.2 Photopolarimetry models and analytic disc warping

The observed photopolarimetric variability in AA Tau has been interpreted as eclipses of the star by a warp in the circumstellar disc. To investigate this interpretation, we have constructed scattered light simulations where we introduce a warp into the axisymmetric disc geometry that we derived from SED fitting. Informed by the dynamical model (Section 4), where the disc mid-plane is not raised and lowered to produce the warp but material piles up at the corotation radius, we create the disc warp by introducing an azimuthal, ϕ, dependence of the disc scaleheight,

$$z_0 = z_w \exp -\frac{1}{2}[(\phi - \phi_0)/\Delta\phi]^2 \exp -\frac{1}{2}[(\varpi - \varpi_0)/\Delta\varpi]^2, \quad (1)$$

with z_w the amplitude of the warp, ϕ_0 the azimuth of the warp and $\Delta\phi$ the azimuthal extent of the warp. The warp is further constrained in radius with the second Gaussian function so that it peaks at ϖ_0 and extends over a radius $\Delta\varpi$. A warp is created in both the positive and negative z directions, with the peaks having a π phase separation. A second warp in the negative z direction does not alter our simulated light curves for this viewing angle. Fig. 2 shows the warp in the inner regions of the disc on the positive z surface responsible for the photopolarimetric variability. Fig. 3 shows the dynamically induced warp in the inner regions of the disc, which is of similar dimensions but has a larger radial extent. As mentioned earlier, the radial extent of the warp has little effect once it is large enough to fully obscure the central source, so this makes no difference to the photopolarimetry of the model.

After the original interpretation that the variability of AA Tau was the result of a warped inner disc (Bouvier et al. 1999), a study by Terquem & Papaloizou (2000) examined the conditions under which an inclined stellar magnetic dipole could reproduce the required warp. They found that a dipole inclined at 30° is easily capable of inducing a warp of the size proposed by Bouvier et al. (1999).

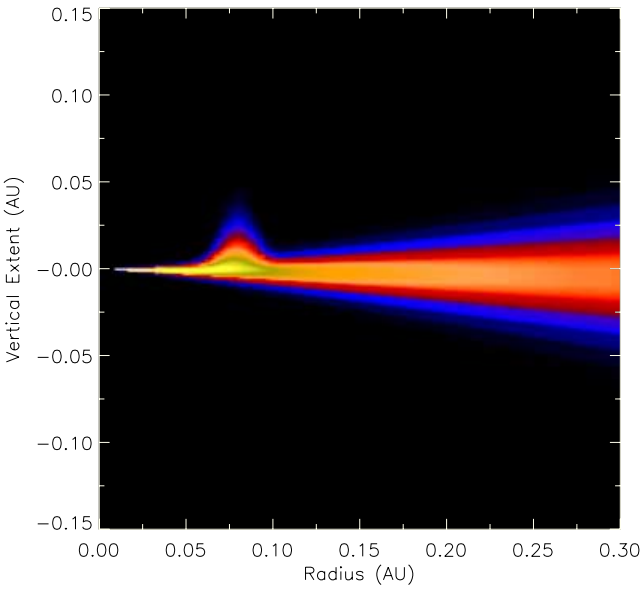

Figure 2. Analytically induced warp used to fit the photopolarimetric variability of AA Tau. The figure shows a slice through the disc density at azimuthal angle $\phi = 0°$, showing the peak amplitude of the inner disc warp.

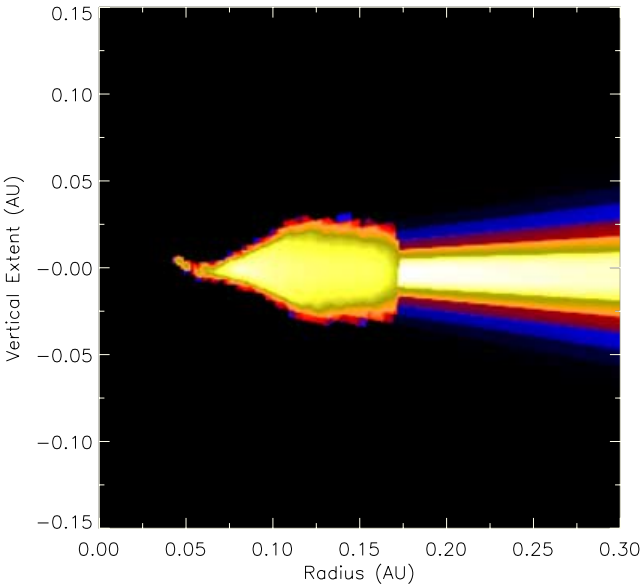

Figure 3. Dynamically induced warp used to fit the photopolarimetric variability of AA Tau. The figure shows a slice through the disc density, showing the peak amplitude of the disc warp.

They also discovered that, depending on the viscosity of the disc, the vertical displacement of the disc varied rapidly (low viscosity) and was likely to cause breakup or caused a smoothly varying warp of the kind expected (high viscosity). Both cases would produce variations in light curves that could possibly be distinguished from one another.

Our parametrized inner disc warp simulations that best reproduce the observed photopolarimetry have $i = 75°$, $z_w = 0.016$, $\Delta\phi = 75°$, $\varpi_0 = 0.072$ au and $\Delta\varpi_0 = 0.0084$ au. Fig. 4 shows the photopolarimetric light curves for this model. Note that the photometric variability for a warped disc is achromatic, as observed. Even

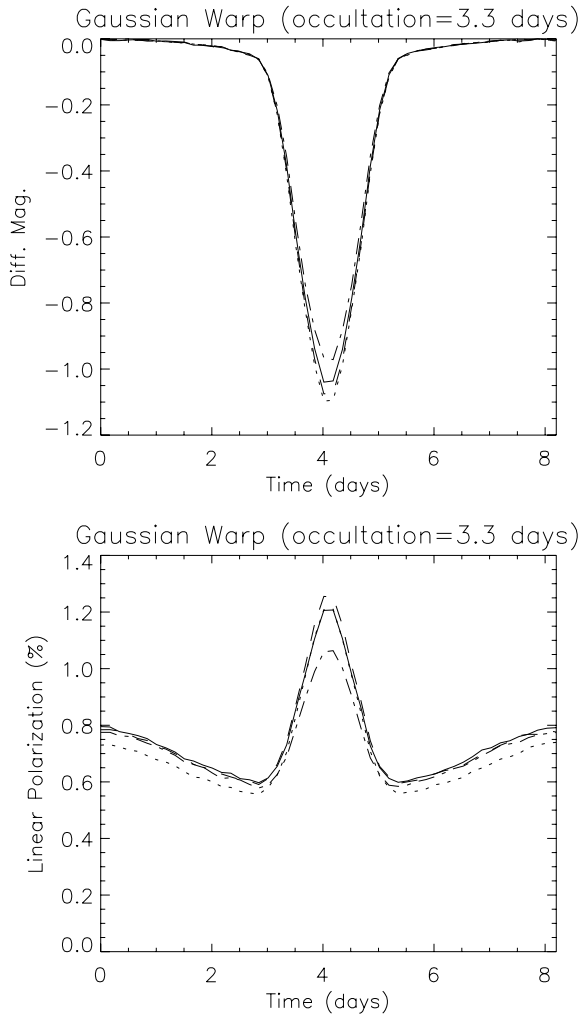

Figure 4. Photopolarimetry simulations of a Gaussian shaped warp with an occultation duration of 3.3 d. The upper panel shows the variation in observed flux, with $\Delta m \sim 1$, for U (dotted), B (dashed), V (solid) and I (dot-dashed) bands. The lower panel shows the corresponding linear polarization with $P = 0.4$–1.05 per cent in the V band.

though there is a wavelength dependence on the circumstellar dust opacity, the disc warp is optically thick enough that colour variations in the photometry are not observable. Slight wavelength-dependent variations are present in the level of polarization. In the observed polarimetry of AA Tau (Bouvier et al. 1999), there is a substantial position angle variation of around 0° to 30°. By comparison with other stars in the vicinity, a study by Menard et al. (2003) attributed this variation to the interstellar medium (ISM). After ISM polarization is removed, the change in position angle, ΔPA, drops to 0°.In our simulations, we find $\Delta PA \sim 4°$ indicating that there is in fact some intrinsic ΔPA. If this is the case, then it is not unreasonable to assume that the interstellar polarization is < 0.5 per cent. The removal of a smaller interstellar polarization component would in turn produce a slightly higher linear polarization value for AA Tau, somewhere between the value stated by Bouvier et al. (1999) and Menard et al. (2003) mentioned earlier.

Clearly many different warped disc models could match the observations and we have constrained the parameters as follows.

The direct stellar flux and polarization from a flared disc are sensitive to the inclination angle (e.g. Whitney & Hartmann 1992). For viewing angles $i > 78°$, the star becomes blocked by the flared disc and the polarization increases dramatically (e.g. see Stassun & Wood 1999; Fig. 5) because the relative fraction of scattered to direct starlight increases. For viewing angles $i < 70°$, we obtain very low polarization values and would require very large warps, z_w, to obtain the observed photometric variability. We do not allow warps to exceed $z_w/\varpi_0 = 0.3$ in accordance with theoretical models of disc warping (Bouvier et al. 1999). The warp must be constrained to a fairly narrow range in disc radius to obtain the observed variability. Warps extending over large radial distances would not survive as a result of differential rotation in the disc. The shape of the photopolarimetry light curve allows us to place constraints on the azimuthal extent of the warp. As the occultation itself is reported to last from 3–4 d, it implies a warp with an azimuthal extent of 130°–175°. The warp in Fig. 4 matches the observed brightness variation and polarization of AA Tau. We find that as we increase the extent of the warp around the disc there is very little change in the brightness variation but there is a reduction in the level of polarization reached during the occultation. Values of $\Delta\phi$ much larger or smaller than what we use result in light curves that show too broad or too narrow an eclipse feature.

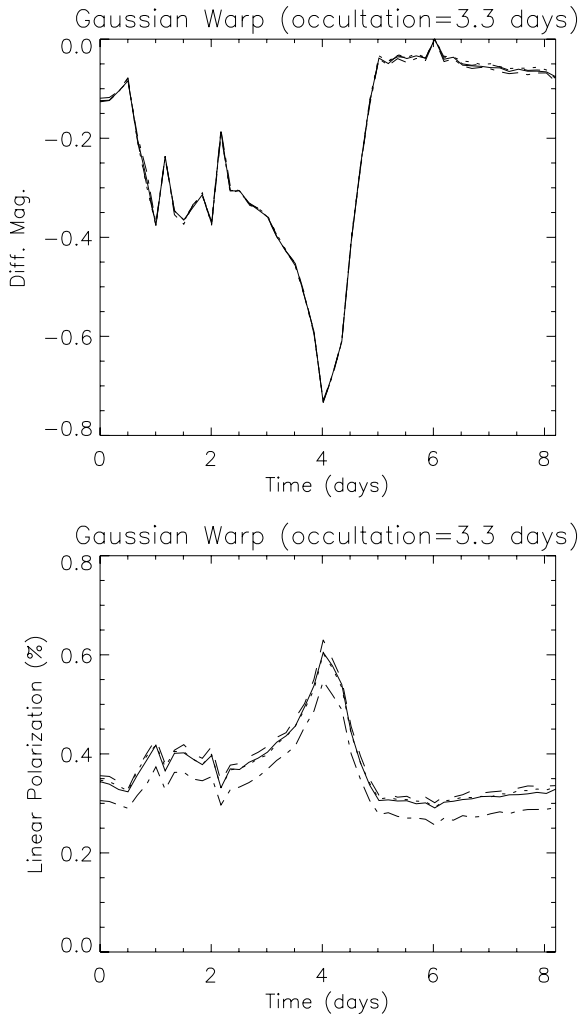

Figure 5. Photometry simulations of the dynamically induced warp with an occultation duration of ∼3 d. The upper panel shows the variation in observed flux, with $\Delta m \sim 0.73$ mag, for U (dotted), B (dashed), V (solid) and I (dot-dashed) bands. The lower panel shows the corresponding linear polarization with $P = 0.6$–0.8 per cent in the V band.

For comparison, modelling was carried out using a sinusoidal shaped warp. The duration of the warp was 3.3 d and there was very little change in the photopolarimetry compared to our previous model. For the sinusoidal warp, $\Delta V = 1.08$ showing good agreement with the Gaussian model ($\Delta V = 1.05$) and the polarization varied from 0.4–1.15 per cent also in good agreement with the Gaussian model where polarization varied from 0.6–1.2 per cent.

Finally we modelled the photopolarimetry of the magnetically induced warp of the dynamical models. A stellar magnetic dipole of 5.2 kG inclined at 30° to the stellar rotation axis produced a warp of approximately the same dimensions as the analytical model. The duration of the occultation event was around 3.3 d with some low-level variability lasting slightly longer. The warp produced a variation in photometry, ΔV, of 0.73 mag. The polarization was found to vary from 0.3–0.6 per cent giving good agreement with the analytical model and the observed variability. Fig. 5 shows the photometric light curves for this model at various wavelengths.

In summary, we estimate the uncertainty in our models to be $i = 75^\circ \pm 2^\circ$, $\Delta\phi = 75^\circ \pm 5^\circ$, $\Delta\varpi = 0.0084 \pm 0.0042$ au and $z_w = 0.016 \pm 0.0016$ au.

3.3 Time sequence scattered light images

In addition to eclipsing the star and producing the observed unresolved photopolarimetric variability, the warp also casts a shadow over the outer regions of the disc. Therefore, a time sequence of high spatial resolution images may detect a shadow sweeping round the disc. Fig. 6 shows a sequence of scattered light images at a range of viewing angles for our AA Tau warped disc model. Fig. 7 shows a series of close-up scattered light images of the warp occulting the star at a viewing angle of 75°. These models may be compared with hot star spot models (Wood & Whitney 1998), which show a lighthouse effect of a bright pattern sweeping around the disc. For some warped disc models, the azimuthal extent of the warp may mimic scattered light images as a result of hot star spots, but multiwavelength photometry can discriminate models: star spots yield chromatic variability, whereas a disc warp yields achromatic photometric variability. Notice that for edge-on viewing the time sequence images for warped discs and discs illuminated by a spotted star (Wood & Whitney 1998) are very similar, and multiwavelength photopolarimetry is required to break the degeneracy.

For completeness, we included in our warped disc models spots of various sizes located at a range of latitudes with a temperature of 8000 K. We found that a spot with an angular radius of 5° was more than enough to visibly alter the photometry at all latitudes causing the wavelength-dependent effects mentioned above. Fig. 8 shows unresolved photopolarimetric models of our warped disc illuminated by a star with hotspots on its surface. The spotted star model exhibits strong colour changes not present in the warped disc model. The shape of both the photometric variation and polarimetric variation curves are also quite different for the spot model purely as a function of the differing geometries involved. These strong colour changes are not reported in AA Tau, however, the HH 30 IRS disc does exhibit a colour dependence (Wood et al. 2000), so it appears that the hotspot models are more appropriate for that system.

4 HYDRODYNAMIC SIMULATIONS

Having analytically investigated the size and shape of the inner disc warping required to match the photopolarimetry of AA Tau, we now use a 3D hydrodynamics code to explore magnetically induced disc warps. We model the inner accretion disc region of AA Tau with a 3D SPH code. SPH is a Lagrangian numerical scheme in which gas

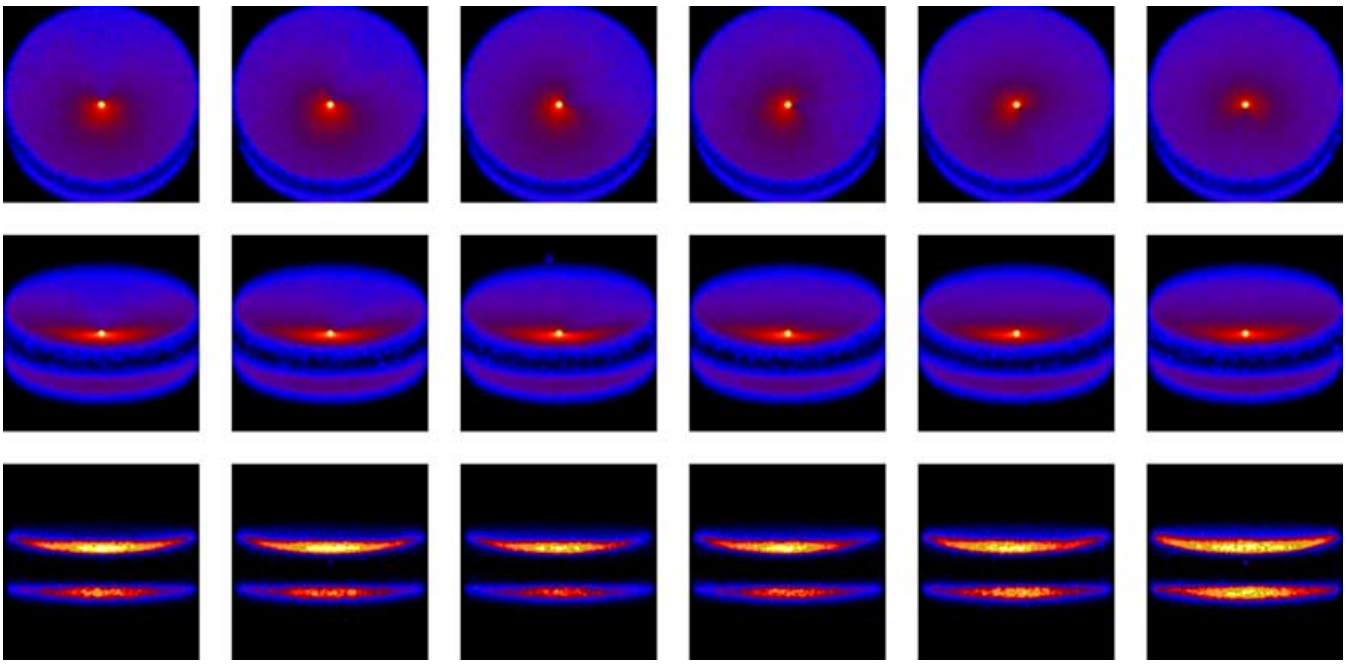

Figure 6. Scattered light images of our warped disc model of AA Tau. The panels on the upper row show the disc at an inclination of 25°, the centre row of panels have inclination 70° and the panels along the bottom show an inclination of 85°, all are 400 au on a side. The images cover half a rotation and clearly show the shadowed area caused by the warp occulting the star moving round the disc. To overcome the large dynamic range between starlight and scattered light in the disc, the images are presented on a one-tenth root (square root for the edge-on disc) stretch. The faintest regions have a surface brightness of 10^{-6} that of the star.

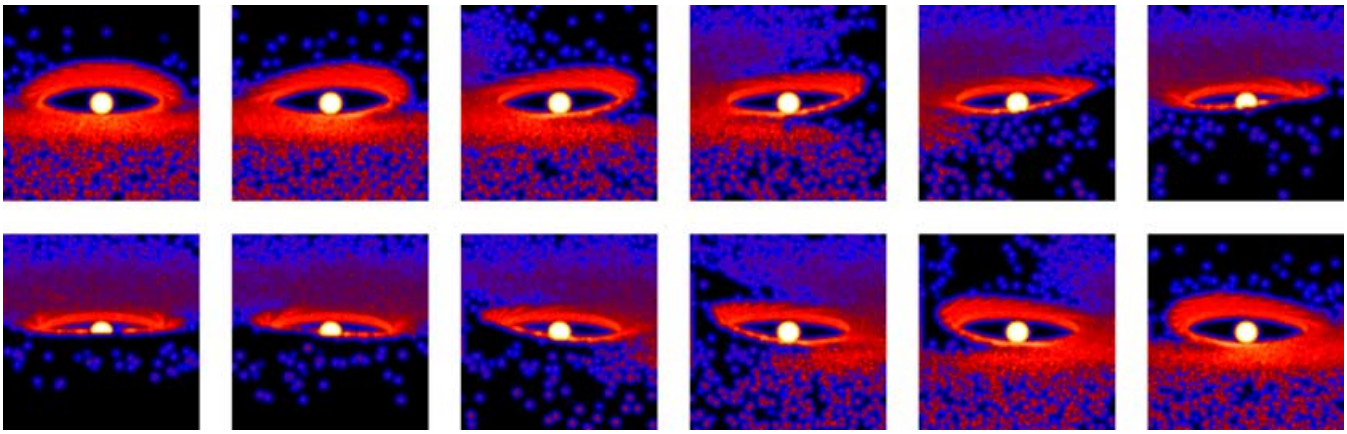

Figure 7. Scattered light images of the warped disc inclined at 75° and with an image diameter of 0.2 *au* clearly showing the material responsible for the photopolarimetric variations occulting the star. To overcome the large dynamic range between starlight and scattered light in the disc, the images are again presented on a one-tenth root stretch. The faintest regions have a surface brightness of 10^{-6} that of the star.

flow is represented by a system of particles moving with the local fluid velocity (Monaghan 1992). The SPH method has been applied successfully to accretion discs in a host of astrophysical situations including protoplanetary discs (Rice et al. 2003), cataclysmic variables (Truss et al. 2000) and microquasars (Truss & Wynn 2004) and has been applied to the magnetic warping of discs by Murray et al. (2002). The warping of a disc in response to an offset dipolar field has also been calculated with a 3D Eulerian magnetohydrodynamics code by Romanova et al. (2003).

In our model, we use operator splitting to solve for the dynamics of the gas flow subject to three forces. The gas pressure force is computed by solving the SPH momentum equation with the standard SPH viscosity term:

$$\frac{\mathrm{d}\mathbf{v}_i}{\mathrm{d}t} = -\sum_j m_j \left(\frac{P_i}{\rho_i^2} + \frac{P_j}{\rho_j^2} + \frac{\beta\mu_{ij}^2 - \alpha\bar{c}_{ij}\mu_{ij}}{\bar{\rho}_{ij}} \right) \nabla_i W_{ij}. \tag{2}$$

Here, W_{ij} is the interpolating kernel between particles i and j, $\bar{c}_{ij}$ is the mean sound speed of the two particles and μ_{ij} is such that

$$\mu_{ij} = \begin{cases} \frac{H\mathbf{v}_{ij}\cdot\mathbf{r}_{ij}}{\mathbf{r}_{ij}^2+0.01h^2} & \mathbf{v}_{ij}\cdot\mathbf{r}_{ij} \leqslant 0 \\ 0 & \mathbf{v}_{ij}\cdot\mathbf{r}_{ij} > 0 \end{cases}, \tag{3}$$

where h is the smoothing length and H is the local scaleheight of the disc. The viscosity parameter α, should not be confused with the Shakura–Sunyaev viscosity parameter, although Murray (1996) has shown that, in three dimensions with $\beta = 0$, the net Shakura–Sunyaev viscosity introduced by this model is

$$\alpha = \frac{1}{10}\alpha_{\mathrm{SPH}}. \tag{4}$$

The gravitational attraction of the star is computed via a simple Runge–Kutta fourth-order integrator. We do not consider the self-gravity of the accretion disc, as we are modelling only a small, low-mass region near the central star. Full MHD is not yet possible with SPH, so a third force is added, representing the drag on each particle as a result of a magnetic dipole field anchored on the star. The dipole field is assumed to corotate with the star, but is offset slightly with the rotational axis.

The magnetic drag force model has been described by Wynn, King & Horne (1997) and was first included in a SPH scheme by Murray et al. (2002) to investigate the magnetic warping of discs in cataclysmic variables. The model has been developed further in a recent paper by Matthews, Speith & Wynn (2004), in which it is used in a 1D model of accretion discs in T Tauri stars. Here, we incorporate these developments into a fully 3D hydrodynamic study of a circumstellar disc. In the model, the magnetic tension force appears as

$$a_{\mathrm{mag}} \sim \frac{B_z^2}{4\pi\rho r_{\mathrm{c}}} \left(\frac{\Omega - \Omega_*}{\Omega} \right), \tag{5}$$

where Ω and Ω_* are the angular velocities of the gas and the star respectively and r_{c} is the local radius of curvature of the magnetic field lines. This is approximated as a fraction of the local scaleheight of the disc,

$$r_{\mathrm{c}} = \zeta H, \tag{6}$$

where $\zeta \leqslant 1$ (Pearson, Wynn & King 1997).

For a dipole of magnetic moment μ, we have

$$B_{\mathrm{z}} = \frac{\mu}{r^3}. \tag{7}$$

The drag force acts in a direction perpendicular to the relative velocity of the gas and the rotating field. It is positive, propelling material away from the star, for all radii $r > R_{\mathrm{co}}$, where R_{co} is the corotation radius. Conversely, gas at radii $r < R_{\mathrm{co}}$ feels a net force towards the star. The functional form of this force term is plotted in Fig. 9. For numerical convenience, we only model the flow of gas outside a radius $R_{\mathrm{min}} = 4R_*$, because close to the star the magnetic drag force becomes very large. This has no impact whatsoever on the resolution of structure in the accretion disc itself, which is truncated well outside this radius.

We set up an initial disc comprising 500 000 SPH particles, extending from the corotation radius $R_{\mathrm{co}} = 8.7R_*$ to $20R_*$, where the stellar radius is taken to be $R_* = 1.3 \times 10^{11}$ cm. The mid-plane of the initial disc is coplanar with the stellar equator and has a surface density profile $\Sigma(r) \propto r^{-1}$. It is flared, with a hydrostatic vertical density profile $\rho(z) = \rho(0)\ \exp(-z^2/2H^2)$, where $\rho(0)$ is the density in the mid-plane and H is the scaleheight c_{s}/Ω. The particles are given radial velocities such that throughout the disc the mass accretion rate is constant at a value $\dot{M} = 7.5 \times 10^{-9}\,\mathrm{M}_\odot\,\mathrm{yr}^{-1}$. Here, we are considering the case of a constant mass accretion rate into the inner regions of the accretion disc. Naturally, it is quite possible to surmise that any variations in mass transfer rate will impact on the

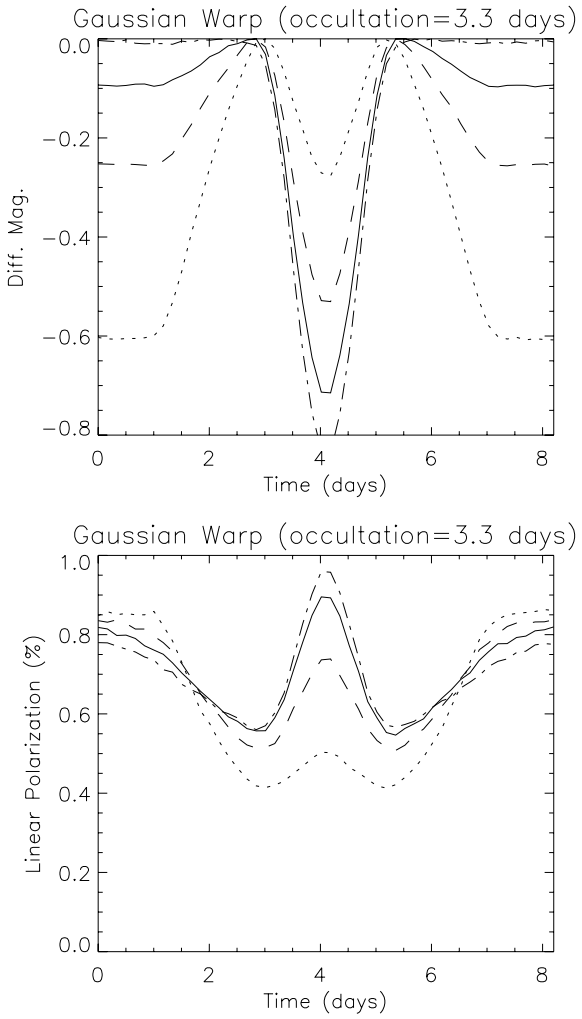

Figure 8. Variations in photometry (top panel) and polarization (bottom panel) for our warped disc illuminated by a spotted star at four different passbands: *U* (dotted), *B* (dashed), *V* (solid) and *I* (dot-dashed). The hotspot is at the same longitude as the warp, is at a latitude of 65°, has a radius of 5° and has a temperature of 8000 K. Note the strong wavelength dependence and different shape of the light curve to that generated by a warped disc geometry.

size and nature of the warping of the disc. This scenario is discussed in a recent paper by Pfeiffer & Lai (2004). We comment that another factor that may affect the long-term behaviour of any warp is magnetic diffusivity, which we do not consider here. It seems likely that a finite resistivity will modify the field structure somewhat, although the importance of this effect for the long-term stability of a disc warp remains unclear.

We use a Shakura–Sunyaev viscosity parameter $\alpha = 0.01$, $\beta = 0$ and a dipole moment $\mu = 1.2 \times 10^{37}$ Gcm^3. With $\zeta = 1$, this corresponds to a stellar field strength $B(R_*) = 5.2$ kG, which is slightly larger than the values usually quoted for T Tauri stars, in the range 2–3 kG. This field was required to produce the warp described below for the parameters given, although it should be stressed that there is nothing to prevent $\zeta < 1$, in which case there is better agreement with the observed field strengths. The magnetic dipole is offset at angle $\pi/6$ to the axis of stellar rotation.

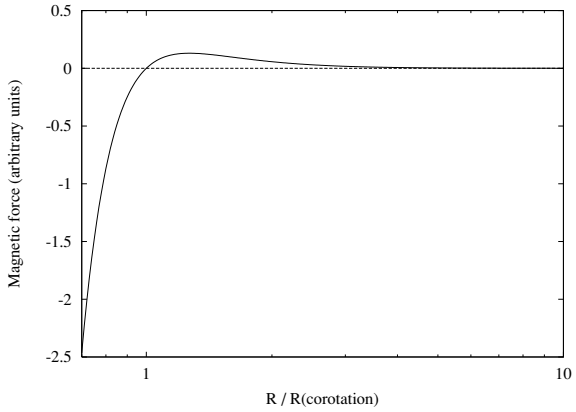

Figure 9. The radial dependence of the magnitude of the magnetic drag acceleration term, plotted here for a surface density profile $\Sigma \sim \rho H \propto 1/r$. In the simulations, the surface density is calculated self-consistently, but in practice departures from this profile are small. The net drag force is directed towards the central star inside the corotation radius and its magnitude increases sharply towards the star. Outside the corotation radius, the net drag force is weaker and is directed away from the central star. The drag force is zero at $R = R_{\rm co}$.

After several orbits under the influence of the magnetic field, a stable warped structure develops near the corotation radius. Fig. 10 shows the local average height of the disc above the mid-plane, in the initial and final states. The warp has a maximum vertical height of $\sim 2R_*$. This result is consistent with the earlier analysis of Terquem & Papaloizou (2000), who computed the steady warped structure of the disc in AA Tau and predicted a similar trailing spiral structure near the corotation radius. We also made a limited study of the effects of changing the tilt angle of the magnetic dipole. Increasing the tilt angle to $5\pi/18$ had little or no effect on the size of the warp and the resultant disc structure was indistinguishable from that obtained in the original simulation.

5 SUMMARY

We have modelled the photopolarimetric variations of the classical T Tauri system, AA Tau. Our results show that a magnetospherically induced warp of the accretion disc at roughly the stellar corotation radius occults the star and reproduces the observed variability. Our SED modelling provides us with estimates of the disc mass and large-scale density structure that are subsequently used in our non-axisymmetric scattered light disc models. Spotted star models exhibit a strong wavelength dependence, which is not observed in the AA Tau system. Our warped disc model shows no wavelength dependence, and can reproduce the occultation period and duration with the required brightness and polarization variations. A feature of the warped disc model is that it produces a shadow that sweeps around the outer disc and this may be detectable with high spatial resolution time sequence imaging.

Using a modified SPH code, we find that a stellar magnetic dipole of 5.2 kG inclined at 30° to the stellar rotation axis may reproduce the required warp amplitude to occult the star and reproduce the brightness variations. The models we have presented are strictly periodic, so do not reproduce the stochastic nature of the lightcurve of AA Tau (Bouvier et al. 2003). However, our models do show that disc warping resulting from the interaction of the stellar magnetic field with the disc can reproduce the amplitude and shape of the occultation events. In the near future, accurate measurements of

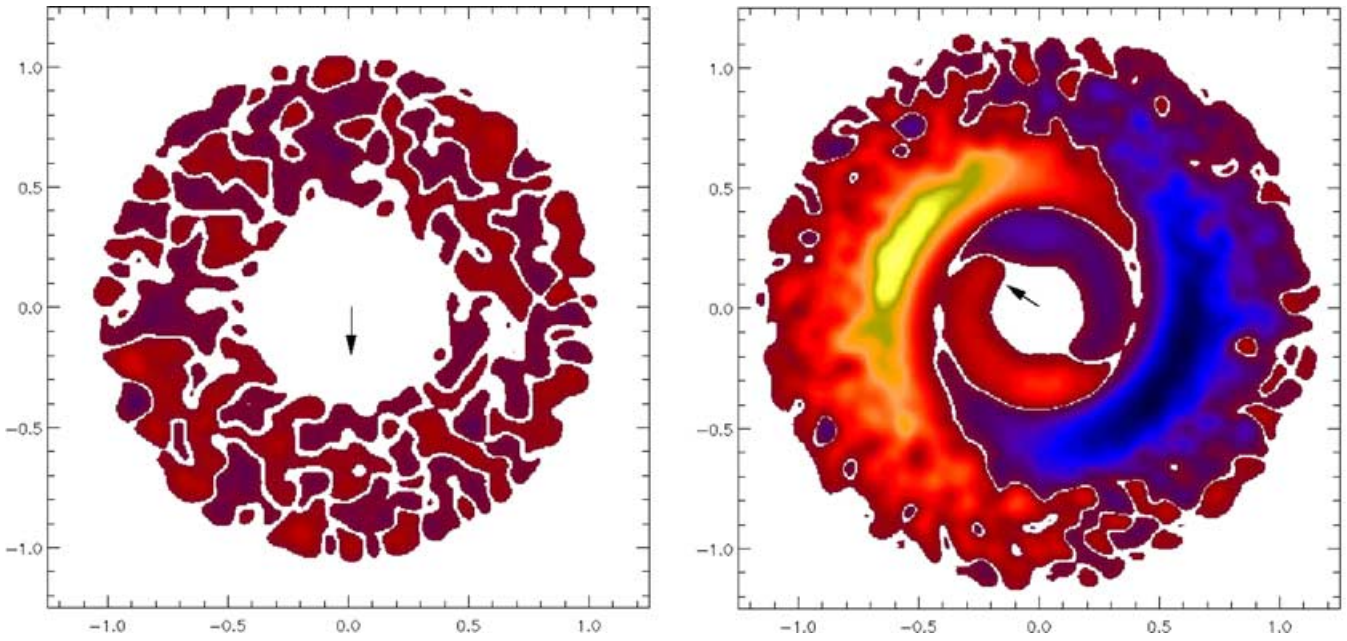

Figure 10. These images of the accretion disc viewed from directly above the star are coloured according to the mean height from the mid-plane at the beginning (left) and end (right) of the simulation. Blue regions are, on average, below the mid-plane, while yellow and orange are, on average, above the mid-plane. Regions that remain coplanar with the stellar equator are left white. The initial conditions (left) are chosen such that the altitude of gas at each radius is symmetric about the mid-plane, hence the mean height appears random (but is very close to zero). The axes are scaled in units of $20R_*$. Gas that appears inside the corotation radius (which lies near 0.45 in these units) is threaded on to the magnetic field lines of the stellar dipole field. The black arrows at the centre of the disc show the projected direction of the north pole of the dipole, which is offset at an angle 30° to the vertical.

the magnetic field structures of T Tauri stars will be possible using Zeeman Doppler imaging (Petit & Donati 2004), allowing more realistic (i.e. non-dipolar) modelling of the stellar magnetic field, its impact on the disc and observational signatures.

ACKNOWLEDGMENTS

We acknowledge financial support from PPARC studentships (MO, CW, OM), a Postdoctoral Fellowship (MT) and an Advanced Fellowship (KW).

REFERENCES

Appenzeller I., Mundt R., 1989, A&AR, 1, 291
Bertout C., 1989, ARA&A, 27, 351
Bjorkman J. E., Wood K., 2001, ApJ, 554, 615
Bouvier J., Cabrit S., Fernandez M., Martin E. L., Matthews J. M., 1993, A&A, 61, 737
Bouvier J. et al., 1999, A&A, 349, 619
Bouvier J. et al., 2003, A&A, 409, 169
Burrows C. J. et al., 1996, ApJ, 473, 437
Chiang E. I., Joung M. K., Creech-Eakman M. J., Qi C., Kessler J. E., Blake G. A., van Dishoeck E. F., 2001, ApJ, 547, 1077
Choi P. I., Herbst W., 1996, AJ, 111, 283
Code A. D., Whitney B. A., 1995, ApJ, 441, 400
Cotera A. et al., 2001, ApJ, 556, 958
D'Alessio P., Calvet N., Hartmann L., Lizano S., Canto J., 1999, ApJ, 527, 893
Dullemond C. P., Dominik C., 2004, A&A, 421, 1075
Eaton N. L., Herbst W., Hillenbrand L. A., 1995, AJ, 110, 1735
Ghosh P., Lamb F. K., 1979, ApJ, 232, 259
Hatzes A. P., 1995, ApJ, 451, 784
Herbst W., Herbst D. K., Grossman E. J., Weinstein D., 1994, AJ, 108, 1906
Joy A., 1945, ApJ, 102, 168
Kenyon S. J., Hartmann L., 1995, ApJS, 101, 117
Kenyon S. J. et al., 1994, AJ, 107, 2153
Koenigl A., 1991, ApJ, 370, L39
Kurucz R. L., 1995, CD-ROM 19, Solar Model Abundance Model Atmospheres. SAO, Cambridge
Matthews O. M., Speith R., Wynn G. A., 2004, MNRAS, 347, 873
Ménard, F., Bouvier J., Dougados C., Melnikov S. Y., Grankin K. N., 2003, A&A, 409, 163
Mhadavi A., Kenyon S. J., 1998, ApJ, 497, 342
Monaghan J. J., 1992, ARA&A, 30, 543
Murray J. R., 1996, MNRAS, 279, 402
Murray J. R., Chakrabarty D., Wynn G. A., Kramer L., 2002, MNRAS, 335, 247
Pearson K. J., Wynn G. A., King A. R., 1997, MNRAS, 288, 421
Petit P., Donati J.-F., 2004, The ESPaDOnS project team, EAS Publication Series, 9, 97
Pfeiffer H. P., Lai D., 2004, ApJ, 604, 766
Rice W. K. M., Wood K., Armitage P. J., Whitney B. A., Bjorkman J. E., 2003, MNRAS, 339, 1025
Romanova M. M., Ustyugova G. V., Koldoba A. V., Wick J. V., Lovelace R. V. E., 2003, ApJ, 595, 1009
Schneider G., Wood K., Silverstone M., Hines D. C., Koerner D. W., Whitney B., Bjorkman J. E., Lowrance P. J., 2003, AJ, 125, 1467
Shakura N. I., Sunyaev R. A., 1973, A&A, 24, 337
Shu F., Najita J., Ostriker E., Wilkin F., Ruden S., Lizano S., 1994, ApJ, 429, 781
Stapelfeldt K. R. et al., 1999, ApJ, 516, L95
Stassun K., Wood K., 1999, ApJ, 510, 892
Terquem C., Papaloizou J. C. B., 2000, A&A, 360, 1031
Truss M. R., Wynn G. A., 2004, MNRAS, 353, 1048
Truss M. R., Murray J. R., Wynn G. A., Edgar R. G., 2000, MNRAS, 319, 467
Walker C., Wood K., Lada C. J., Robitaille T., Bjorkman J. E., Whitney B. A., 2004, MNRAS, 351, 607
Watson A. M., Stapelfeldt K. R., 2004, ApJ, 602, 860
Whitney B. A., Hartmann L., 1992, ApJ, 395, 529

Whitney B. A., Wood K., Bjorkman J. E., Cohen M., 2003, ApJ, 598, 1079
Wood K., Whitney B. A., 1998, ApJ, 506, L43
Wood K., Kenyon S. J., Whitney B. A., Bjorkmann J. E., 1996, ApJ, 458, L79
Wood K., Stanek K. Z., Wolk S., Whitney B., Stassun K., 2000, AAS, 32, 1414
Wood K., Lada C. J., Bjorkman J. E., Kenyon S. J., Whitney B. A., Wolff M. J., 2002, ApJ, 567, 1183
Wynn G. A., King A. R., Horne K. D., 1997, MNRAS, 286, 436

This paper has been typeset from a TEX/LATEX file prepared by the author.